Neutral Alkaline-Metal and Alkaline-Earth-Metal Derivatives of Imidazole and Benzimidazole

ARTICLE *in* THE JOURNAL OF PHYSICAL CHEMISTRY A · JUNE 2014

Impact Factor: 2.69 · DOI: 10.1021/jp502443h

4 AUTHORS:

Fernando Blanco

European University of Madrid

68 PUBLICATIONS **1,206** CITATIONS

SEE PROFILE

David Lloyd

Trinity College Dublin

69 PUBLICATIONS **1,036** CITATIONS

SEE PROFILE

Ibon Alkorta

Spanish National Research Council

680 PUBLICATIONS **12,430** CITATIONS

SEE PROFILE

José Elguero

Spanish National Research Council

1,502 PUBLICATIONS **22,206** CITATIONS

SEE PROFILE

THE JOURNAL OF PHYSICAL CHEMISTRY A

Article

pubs.acs.org/JPCA

Neutral Alkaline-Metal and Alkaline-Earth-Metal Derivatives of Imidazole and Benzimidazole

Fernando Blanco,[†] David G. Lloyd,[†,§] Ibon Alkorta,*[,‡] and José Elguero[‡]

[†]Molecular Design Group, School of Biochemistry and Immunology, University of Dublin, Trinity College, Dublin 2, Ireland

[‡]Instituto de Química Médica, CSIC, Juan de la Cierva, 3, E-28006 Madrid, Spain

[§]Division of Health Sciences, University of South Australia, Adelaide, SA 5000, Australia

Supporting Information

ABSTRACT: A theoretical study of the minima and connecting transition states of the neutral complexes formed by alkaline-metal and alkaline-earth-metal derivatives of imidazolate and benzimidazolate anions has been carried out using B3LYP/6-31+G(d,p), B3LYP/6-311+G(3df,2p), and G3B3 methods. Two and three nondegenerated minima and two and four TS structures have been identified for imidazole and benzimidazole derivatives, respectively. The most stable minima of the alkaline-metal derivatives of both systems correspond to the metal interacting with the imidazole ring, whereas in the alkaline-earth-metal derivatives, the preferred minima depend on the substituent. A remarkable feature of some minima is the fact that some of the metal−aromatic interactions follow the classical π−cation pattern, even though the global structure corresponds to a neutral salt, constituting a class of noncovalent interaction of great interest in the chemistry of aromatic and heterocyclic complexes. A CSD search has confirmed that the two bonding modes, N−σ and π, are present in the solid phase. The π mode has been analyzed by comparison with other azoles.

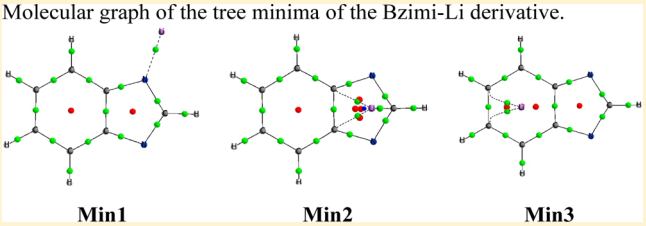

1. INTRODUCTION

In recent years a number of publications have focused on the study of interactions between charged groups and aromatic systems, due to the importance of understanding the mechanism of action of a number of biological systems[1] and its interest in the fields of supramolecular structures[2,3] and new materials.[4]

Imidazole (Im) is a heterocyclic system that is incorporated as a side chain in the amino acid histidine[5] and in the neurotransmitter histamine.[6] Among the important functions of histidine is its binding to the Fe(II/III) of hemoglobin.[7] Decarboxylation of histidine produces histamine. Benzimidazole (Bzim) is present in the vitamin B12 structure, coordinated to a central Co(II).[8] Other metals of biological relevance also show interactions with imidazole and benzimidazole such as Cu(II), Zn(II), Cd(II), etc.[9] Beyond the biological sphere these heterocycles are important in systems such as ionic liquids[10] and Arduengo's carbenes.[11]

Recent experimental[12,13] and theoretical[14,15] studies on neutral alkaline-metal complexes of pyrazoles, an isomer of imidazole, have shown the presence of two minima, one with the metal linked to the nitrogen atom (pyridine-like N atom, σ-complex) and another above the five-membered ring (π-complex). These two minima are conceptually analogous to the tautomers found in heterocycles but with the moving moiety being a lithium atom (lithium tautomerism) instead of a proton (prototropic tautomerism). In the pyrazole derivatives, the tautomers with the metal linked to the nitrogen atom were between 16 and 39 kJ mol^{-1} more stable than those with the metal interacting with the π-system, at the MP2 computational level.[12] The referred metal π-derivatives constitute a differentiated class from the best-known class of metal π−cation complexes in the family of weak interactions.[16] The uncharged character of the global system (a neutral salt) is the consequence of the interaction between a positive charged metal with the aromatic region of a deprotonated heterocycle, such as imidazolate (Figure 1).

In our previous articles, a systematic characterization of the N−σ vs the π structure minima of the alkaline-metal derivatives of azoles was carried out. It was observed that in those azoles where no adjacent nitrogen atoms are present (pyrrole and imidazole), the most stable structure is the π one whereas in the less stable one it was the N−σ one.[14] In addition, mono- and bispyrrole and imidazole derivatives of alkaline-earth metals have been also studied.[15] These systems show a positive charge in the case of the mono derivatives and a neutral one in the case of the bis derivatives. The results indicate that, in the mono derivatives, the π configuration is favored for all the systems considered, whereas, in the bis compounds, only the calcium derivatives show the π−π configuration as the calculated absolute minimum.

In the present article, the stationary points (minima and transition state) of the alkaline- and alkaline-earth-metal neutral derivatives of imidazole and benzimidazole have been

Received: March 11, 2014
Revised: May 20, 2014
Published: May 20, 2014

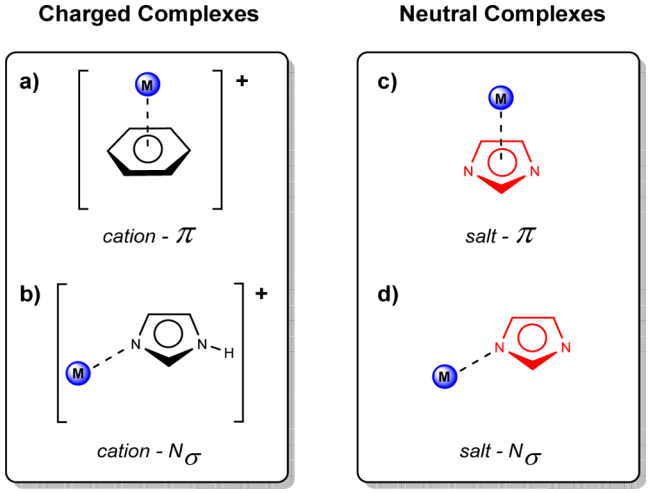

Figure 1. Schematic representation of the classical metal−π interaction and the neutral derivatives studied in the present article.

characterized. Subsequently, the electronic properties of the minima and TS have been analyzed and discussed by means the NBO and AIM methodologies.

2. METHODS

The initial geometry of the structures was fully optimized using B3LYP/6-31+G(d,p) within the Gaussian-03 package.[17] Further geometry optimizations were carried out at B3LYP/6-311+G(3df,2p) and G3B3 computational levels.[18] G3B3 is a variant of the G3 theory where the geometry and zero point energy are calculated at B3LYP/6-31G* level. Additional calculation at MP2 and MP4 levels with large basis sets are carried out in the G3B3 method to obtain accurate values of the energy. It was not possible to carry out G3B3 calculations for the K and Ca derivatives as there are no available basis sets for these elements. Frequency calculations were carried out at the corresponding computational level to confirm that the structures obtained correspond to energetic minima or true transition state (zero and only one imaginary frequencies, respectively). The stability of the wave function was confirmed at the B3LYP/6-31+G(d,p) computational level.

The triplet electronic configuration of the imidazole minima was calculated at the B3LYP/6-31+G(d,p) and showed high relative energy when compared to the corresponding singlet configuration. Thus, they have not been considered in the present article. The topological properties of the electron density were studied using the atoms in molecules (AIM) methodology.[19] The AIMPAC,[20] AIM2000,[21] and AIMAll[22] programs were used to carry out these calculations.

To characterize the aromaticity of the different structures found, two aromaticity indexes were calculated. The HOMA index[23] is geometry-based and can be obtained from bond lengths using the equation: HOMA = $1 - [(\alpha/n)\sum(R_{opt} - R_i)^2]$, where R_{opt} and R_i are optimal bond lengths and bond lengths in the real system, respectively. The variable α is an empirical factor that provides a value of HOMA equal to 0 for the Kekulé structure of benzene and a value of 1 for benzene with optimal "aromatic" bond lengths. Finally, n is the number of bonds considered. The second index considered corresponds to the NICS, which is defined as the negative absolute magnetic shielding computed in the center of the ring.[24] The NICS(1) index was calculated at 1 Å above the ring center.[25]

A search in the CSD[26] (Version 5.34, with the updates of Nov-2012, Feb-2013 and May-2013) was carried out to find alkaline- and alkaline-earth-metal imidazole derivatives with configurations similar to those reported here.

3. RESULTS AND DISCUSSION

3.1. Imidazole Derivatives. Structures of the imidazole derivatives are shown in Figure 2 with their corresponding symmetry and the energetic results reported in Table 1. The geometry of the stationary points calculated at the B3LYP/6-31+G(d,p) and B3LYP/6-311+G(3df,2p) levels are presented in the Supporting Information (Table S1). In general, similar trends are evidenced across all the computational methods.

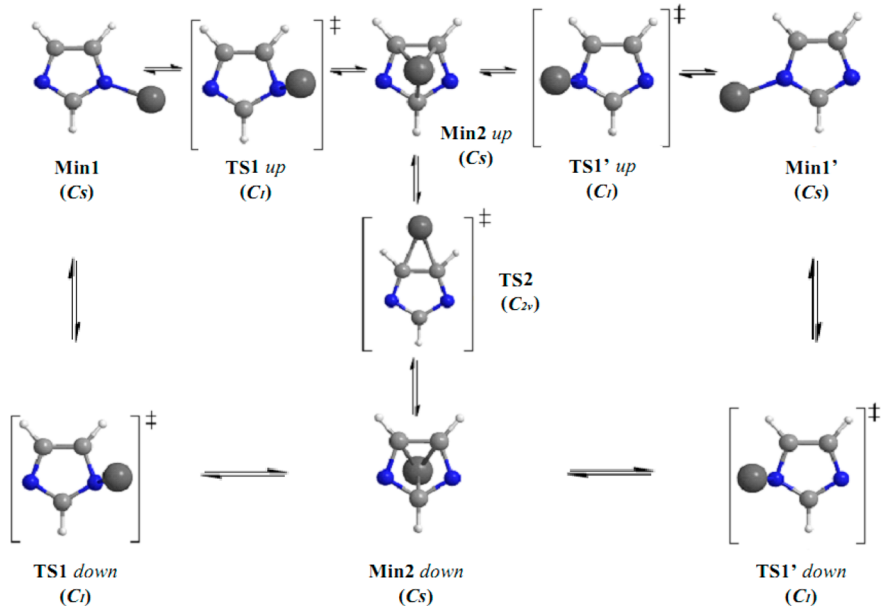

Figure 2. Minima and connecting TS characterized for the lithium−imidazole molecule. For completeness, the mirror images of **Min1**, **TS1**, and **Min2** (**Min1**′, **TS1** *up*, **TS1**′ *up/down*, and **Min2** *down*) have been added to the figure.

dx.doi.org/10.1021/jp502443h | J. Phys. Chem. A 2014, 118, 4195−4204

Table 1. Relative Enthalpy, H_{rel}, and Free Energies, G_{rel} (kJ mol^{-1}), of the Imidazole Structures Considered[a]

		B3LYP/6-311+G(3df,2p)			G3B3	
complex	geometry	H_{rel}	G_{rel}	BDE	H_{rel}	G_{rel}
Imi···Li	**Min1**	30.9	24.6	609	37.2	29.7
Imi···Li	**Min2**	0.0	0.0	640	0.0	0.0
Imi···Li	**TS1**	36.3	35.0		40.8	38.2
Imi···Li	**TS2**	139.1	141.4		146.4	148.5
Imi···Na	**Min1**	17.7	11.6	517	29.2	28.4
Imi···Na	**Min2**	0.0	0.0	534	0.0	0.0
Imi···Na	**TS1**	17.8	17.2		29.2	28.2
Imi···Na	**TS2**	118.3	122.4		126.5	130.3
Imi···K	**Min1**	29.5	20.5	445		
Imi···K	**Min2**	0.0	0.0	474		
Imi···K	**TS1**	27.3	25.8			
Imi···K	**TS2**	110.9	114.9			
Imi···BeH	**Min1**	0.0	0.0	1022	0.0	0.0
Imi···BeH	**Min2**	55.2	59.4	966	31.9	36.4
Imi···BeH	**TS1**	63.7	68.9		48.2	53.6
Imi···BeH	**TS2**	221.7	227.6		216.6	222.3
Imi···MgH	**Min1**	0.0	0.0	758	4.1	0.0
Imi···MgH	**Min2**	13.1	17.3	745	0.0	0.5
Imi···MgH	**TS1**	20.6	26.8		16.5	18.7
Imi···MgH	**TS2**	175.8	183.2		174.6	177.8
Imi···CaH	**Min1**	39.5	32.3	624		
Imi···CaH	**Min2**	0.0	0.0	664		
Imi···CaH	**TS1**	38.5	36.8			
Imi···CaH	**TS2**	163.1	164.7			

[a]The heterolytic bond dissociation enthalpies (kJ mol^{-1}), BDE, for imidazole−metal are also included.

Excellent linear correlations were obtained especially between the two B3LYP levels for both H_{rel} and G_{rel} (slopes close to 1.0, small intercepts and R^2 larger than 0.996). Accordingly, only the values for the larger basis set, 6-311+G(3df,2p), will be reported in the body of the article.

3.1.1. Geometry and Energy Analysis. Optimization of the geometries afforded only two minima, one with the metal atoms interacting with the nitrogen atom (**Min1**) and the other one interacting with the π-cloud (**Min2**). The energetic results obtained at B3LYP and G3B3 follow similar trends. However, in all cases, the relative energies between **Min 1** and **Min2** calculated at the G3B3 level favor **Min2** when compared to those of the same systems calculated at the B3LYP level. Similar differences have been described between MP2, which is the basis of the G3B3 energy, and B3LYP methods.[27−29]

The energetic analysis reveals **Min2** as the most stable minimum in the case of the alkaline metals (Li, Na, and K) and in one case of the alkaline-earth-metal derivatives (CaH). Oppositely, in the case of BeH and MgH, the configuration with the metal atom bonded to the annular nitrogen (**Min1**) is more stable at all levels, with the only exception of MgH at G3B3 level where the two minima show similar energies.

An analysis of the heterolytic bond dissociation enthalpies, BDE, of the azole−metal bond shows that a larger dissociation energy is found in the beryllium derivative followed by the magnesium one. These two cases are the ones associated with a larger stabilization of **Min 1** vs **Min2**. In the rest of the cases, **Min 2** is favored vs **Min 1**. Thus, it seems that those cases with the larger stabilizations favor the nitrogen−metal interaction vs the π-metal one.

A TS has been found connecting **Min1** with **Min2** (**TS1**) and another TS connecting the two degenerate **Min2** structures above and below the plane of the imidazole ring (**TS2**). **TS1** shows relative energies slightly larger than those of the less stable minimum configuration. In contrast, the barriers described by the **TS2** are very large, their relative energy ranging between 110 and 227 kJ mol^{-1}, suggesting that the most favorable path to interconnect the two degenerate **Min2** is through **TS1** and **Min1**.

3.1.2. NBO Analysis. Analysis of the NBO charges provides a general description of the electronic interaction between the metal/heteroaromatic partners in the complexes (Table 2). As shown, in all cases the metallic fragments (M in the alkaline-metal derivatives and MH in the alkaline-earth-metal ones) present charges below +1, evidencing an effective displacement of electronic density from the imidazole moieties to the metal. The observed charges in the metallic fragments are always larger in **Min1** than in **Min2**. These differences are larger in the alkaline-earth-metal derivatives than in the corresponding alkaline-metal ones. In addition, the larger differences are found in the derivatives of the smaller metallic atoms decreasing as its size increases. In both alkaline- and alkaline-earth-metal complexes, this charge transfer, ΔQ, is more effective as the atomic number of the metal involved is lower ($\Delta Q_{Li} > Q_{Na} > \Delta Q_K$ and $\Delta Q_{BeH} > \Delta Q_{MgH} > \Delta Q_{CaH}$, respectively) and always in a narrow range. These results could be rationalized in terms of the higher polarizability of the metallic moieties as their size increases, which allows them to better accommodate the positive charge. More significant are the differences between the metals of the same row in the periodic table. There, the charge transfer of complexes involving alkaline-earth metals is clearly higher than those obtained for the corresponding alkaline-metal ones ($\Delta Q_{Be} \gg \Delta Q_{Li}$, $\Delta Q_{Mg} \gg \Delta Q_{Na}$, and $\Delta Q_{Ca} \gg \Delta Q_K$). The larger electropositive values of the alkaline metals vs those of the alkaline-earth metals, in the same row of the periodic table, are in accordance with the charge transfer tendency previously mentioned.

Table 2. NBO Total Charges (e) of the Metal (Li, Na, and K) or Metal−H (Be, Mg, and Ca) in the Complexes and Absolute Charge Transfer (ΔQ) between Imidazole/Metal Subunits Calculated at the B3LYP/6-31+G Computational Level**

complex	geometry	charge M/MH subunit[a]	ΔQ
Imi···Li	**Min1**	0.93	0.07
Imi···Li	**Min2**	0.80	0.20
Imi···Na	**Min1**	0.93	0.07
Imi···Na	**Min2**	0.90	0.10
Imi···K	**Min1**	0.96	0.04
Imi···K	**Min2**	0.94	0.06
Imi···BeH	**Min1**	0.71	0.29
Imi···BeH	**Min2**	0.46	0.54
Imi···MgH	**Min1**	0.82	0.18
Imi···MgH	**Min2**	0.74	0.26
Imi···CaH	**Min1**	0.91	0.09
Imi···CaH	**Min2**	0.85	0.15

[a]Due to the neutral character of the complexes, the total charge of the imidazolates is the same as that of the corresponding metal but in negative values.

dx.doi.org/10.1021/jp502443h | J. Phys. Chem. A 2014, 118, 4195−4204

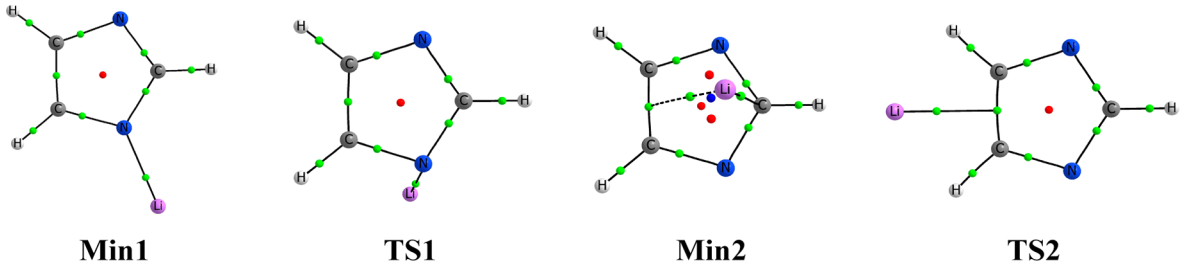

Figure 3. Molecular graph of the stationary structures of the lithium derivative. Green, red, and blue dots represent bond (bcp), ring (rcp), and cage (ccp) critical points, respectively.

The second-order perturbation analysis (Table S2 of the Supporting Information) of the charge transfer between occupied and empty orbitals shows that in **Min1** the charge transfer occurs between the lone pair of the nitrogen atom involved in the interaction and an empty s orbital of the metal atom. The stabilization obtained can be as large as 231 kJ mol^{-1}, as evidenced in the beryllium derivative. In the case of **Min2**, the charge transfer happens between several of the bonds of the ring. In this case, the C−C bond affords the most important contribution to the stabilization energy. Again, the beryllium derivative presents the largest energies, with a maximum of 307 kJ mol^{-1} for the interaction between the C−C bond and one of the empty orbitals of the metallic atom.

The calculated bond indices between the metallic atoms and the atoms of the ring are presented in Table S3 of the Supporting Information. In the case of **Min1**, the bond indices between the nitrogen atoms and the alkaline metals are very small (between 0.11 and 0.06) whereas those in the alkaline-earth-metal derivatives are larger (0.46, 0.27, and 0.14 for the Be, Mg, and Ca derivatives, respectively). In the case of **Min2**, all atoms of the ring have similar bond indices to the metal atom, being slightly larger for the N-metal ones than the C-metal. As previously observed, the values obtained for the alkaline-earth-metal derivatives are larger than those of the alkaline-metal ones, reaching a sum of the indices of 0.97 for the beryllium derivative.

3.1.3. Electronic Analysis. Topological analysis of the electron density of the structures presents a different pattern for each of the stationary points found (see Figure 3 for the stationary points of the lithium derivative and Table S1 of the Supporting Information for all the compounds). With the lithium complexes as an example, the picture shows a simple interaction through the metal and one of the imidazole nitrogen atoms for **Min1** and **TS1**. **Min2** presents a bifurcated path connecting the metal with the carbon C1 and the bond critical point corresponding (bcp) to the covalent C3C4 bond. The corresponding ring (rcp) and cage (ccp) critical points are also apparent. **TS2** presents a different pattern, connecting the Li metal with the C3C4 bcp by a single path. The molecular graphs of the **Min2** and **TS2** structures for the Na, K, Mg, and Ca derivatives show a different topology with two bcps between the metal atoms and the C3 and C4 atoms instead of a single one as observed for the Li and Be derivatives. The electron density at the bcps of metal−N/C atoms of the imidazole ring ranges between 0.118 and 0.014 au (Table S4 of the Supporting Information). The largest electron density is found in the N−metal bond of **Min1** for all complexes. In addition, values are larger in the alkaline-earth-metal derivatives than in the corresponding alkaline-metal analogues. Another interesting feature of the values of the electron density at the bcps is that they are larger for the smaller metal atoms and decrease as the size of the metal atoms increases. For instance the values for the N-metal in **Min1** are 0.050, 0.038, and 0.031 au for the Li, Na, and K series, respectively.

The Laplacian at the metal−N/C bond present always positive values, ranging between 0.059 and 0.062 au. Thus, these bonds can be classified as closed shell interactions, typical of ionic bonds. An additional parameter used to characterize the nature of the bond has been the value of the total electron density, *H*, at the bcp. The values of *H* are always positive except for the beryllium derivatives, which show negative but small values of this parameter. These results reinforce the conclusion that these bonds are mostly ionic with a small covalent contribution.

ELF shows a very similar electronic distribution in the imidazole ring for the parent imidazole derivative, the anion and the two metallic derivative minima found (Figure 4). A

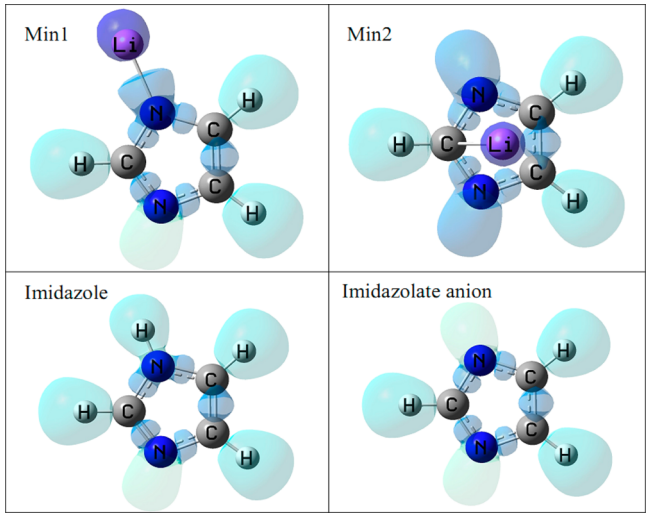

Figure 4. ELF isosurface at 0.75 for the two minima of the Imi···Li, parent imidazole, and imidazolate anion.

quantitative measurement of the perturbation in the electron distribution of the imidazole due to the replacement of the hydrogen atom by a metallic group can be obtained measuring the aromaticity of the ring with the NICS(1) and HOMA parameters (Table 3). In the case of **Min2**, the NICS(1) has been calculated in the opposite face to that where the atomic moiety is located. The values obtained for the two minima species are similar to those of the unsubstituted imidazole (−10.6 and +0.883) and the imidazole anion (−10.9 and +0.928) with the exception of the HOMA value of **Min1** of the

dx.doi.org/10.1021/jp502443h | J. Phys. Chem. A 2014, 118, 4195−4204

Table 3. NICS(1) and HOMA Aromaticity Indexes of the Imidazole Derivatives

	Min1		Min2	
	NICS	HOMA	NICS	HOMA
Imi···Li	−11.0	0.887	−11.6	0.899
Imi···Na	−11.0	0.905	−10.9	0.903
Imi···K	−11.1	0.912	−11.5	0.916
Imi···BeH	−10.6	0.793	−11.9	0.875
Imi···MgH	−11.0	0.855	−10.9	0.879
Imi···CaH	−11.2	0.876	−11.7	0.900
Imi···H	*−10.6*	0.883		
Imi (anion)	*−10.9*	0.928		

beryllium derivative that shows a smaller value that the rest of the derivatives.

The molecular electrostatic potential (MEP) of the **Min1** tautomer shows a significant increment of the negative region surrounding the unsubstituted nitrogen atom whereas in **Min2** the values of the MEP are analogous to those found in the parent imidazole, as shown in Figure 5. The effect observed in the MEP of **Min1** increases the nucleophilicity of the noninteracting nitrogen atom. A similar effect has been reported in the case of beryllium-bonded complexes of imidazole.[30,31]

3.2. Benzimidazole Derivatives. *3.2.1. Geometry and Energy Analysis.* Structures of the optimized benzimidazole derivatives are shown in Figure 6 (the geometry of all the stationary points are reported in Table S1 of the Supporting Information) and their corresponding energetic results reported in Table 4. Three nondegenerate minima were found for most of the benzimidazole derivatives, two of them (**Min1** and **Min2**) are analogous to those found in the imidazole ring. The third (**Min3**) corresponds to the interaction of the metal subunit with the π-cloud of the phenyl ring of the benzimidazole. In alkaline-metal complexes, the energy difference between **Min1** and **Min2** is very small for Li and Na derivatives, although always favoring **Min2**. **Min3** shows higher values of the relative energy, always above 10.0 kJ mol^{-1}. For K complexes, the relative energy clearly favors **Min2**, noting that in this case the structure corresponding to **Min3** does not constitute a stable minimum, evolving toward **Min2**. Closely related to what we have reported for the imidazole series, the BeH and MgH complexes show a clear preference for the N−σ (**Min1**) against the π-aromatic ones (**Min2** and **Min3**), being in the case of BeH derivatives clearly more pronounced. For CaH, as observed before, this situation reverses, with **Min2** becoming the most stable with a narrow but significant margin. Moreover, by analogy with K structures, the aforementioned **Min3** is not stable evolving toward the geometry of **Min2**.

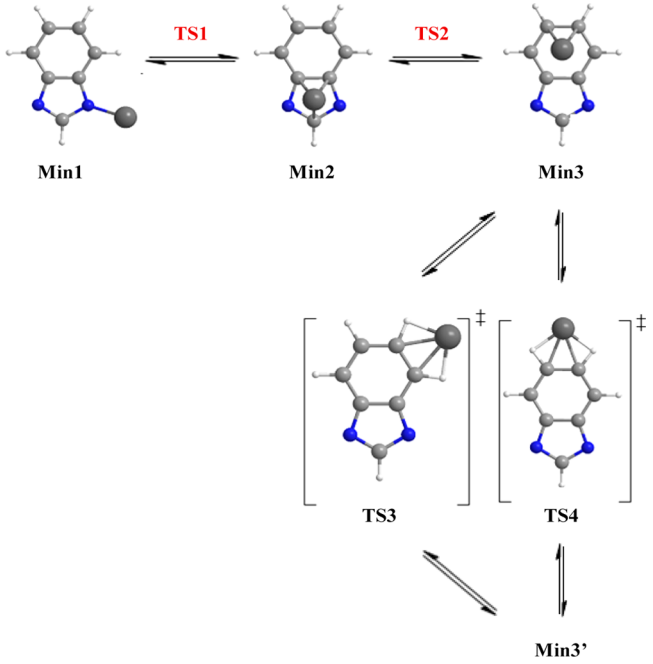

Figure 6. Stationary point in the lithium derivative of benzimidazole.

Four different transition states were localized connecting the three previously mentioned minima. **TS1** is analogous to that described for imidazole series and connects **Min1** and **Min2**. **TS2** connects the π-imidazole and π-phenyl minima (**Min2** and **Min3**) of the benzimidazole ring and is located approximately above the common CC bond (C3a−C7a) of the two rings of the benzimidazole. **TS3** and **TS4** connect two degenerated minima above and below the phenyl ring, **Min3** and **Min3′**. As in the case of the imidazole derivatives, **TS1** presents the smallest barrier and is only slightly larger and less stable than the two connecting minima (**Min1** and **Min2**). In general, **TS2** is about 20 kJ mol^{-1} larger than **TS1** for the same system. Finally, **TS3** and **TS4** show very large values, always larger than 135 kJ mol^{-1} and in some cases up to 280 kJ mol^{-1}.

The values of the heterolytic BDE are about 25 kJ mol^{-1} smaller than the ones obtained for the corresponding imidazole derivatives. This gives some indication that the negative charge is better stabilized in the benzimidazolate system than in the imidazolate one, as expected. As in the previous anlyses, those cases with the largest BDEs (BeH and MgH) are the ones where **Min1** is more stable than **Min2**. However, in the rest of the cases, the preference between **Min1** and **Min2** cannot be explained on the basis of their BDE values.

3.2.2. NBO Analysis. The NBO charges (Table 5) follow a trend similar to that reported for imidazole complexes (Table

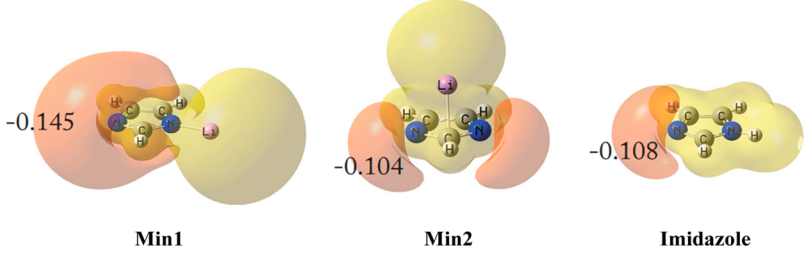

Figure 5. MEP of the lithium derivatives of imidazole, **Min1** (left) and **Min2** (center), and imidazole (right) at ±0.04 au isosurfaces. The values of the MEP minima (au) associated with the lone pairs of the nitrogen are indicated.

dx.doi.org/10.1021/jp502443h | J. Phys. Chem. A 2014, 118, 4195−4204

Table 4. Relative Enthalpy, H_{rel}, and Free Energies, G_{rel} (kJ mol^{-1}), of the Structures Considered for the Benzimidazole Derivatives[a]

		B3LYP/6-311+G(3df,2p)			G3B3	
complex	geometry	H_{rel}	G_{rel}	BDE	H_{rel}	G_{rel}
Bzim···Li	**Min1**	4.8	0.0	580	13.9	7.6
Bzim···Li	**Min2**	0.0	0.8	585	0.0	0.0
Bzim···Li	**Min3**	14.7	16.0	570	18.1	18.4
Bzim···Li	**TS1**	15.5	17.1		19.1	20.3
Bzim···Li	**TS2**	39.2	39.8		38.8	39.0
Bzim···Li	**TS3**	159.8	161.6		172.3	173.3
Bzim···Li	**TS4**	169.0	172.4		182.2	184.6
Bzim···Na	**Min1**	1.6	0.0	491	13.6	15.5
Bzim···Na	**Min2**	0.0	4.9	493	0.0	0.0
Bzim···Na	**Min3**	13.2	18.4	479	15.2	14.8
Bzim···Na	**TS1**	4.75	13.31		10.9	14.5
Bzim···Na	**TS2**	12.9	21.6		14.0	18.2
Bzim···Na	**TS3**	143.6	151.6		157.4	160.3
Bzim···Na	**TS4**	154.2	164.0		168.3	172.6
Bzim···K	**Min1**	16.1	19.3	424		
Bzim···K	**Min2**	0.0	0.0	440		
Bzim···K	**Min3**	*b*	*b*			
Bzim···K	**TS1**	*c*	*c*			
Bzim···K	**TS2**	*b*	*b*			
Bzim···K	**TS3**	137.1	140.4			
Bzim···K	**TS4**	148.3	153.6			
Bzim···BeH	**Min1**	0.0	0.0	988	0.0	0.0
Bzim···BeH	**Min2**	93.0	96.1	895	66.1	69.3
Bzim···BeH	**Min3**	116.4	120.0	871	91.2	95.0
Bzim···BeH	**TS1**	93.3	98.8		70.6	76.2
Bzim···BeH	**TS2**	162.2	165.3		143.8	146.8
Bzim···BeH	**TS3**	274.1	277.8		274.0	277.2
Bzim···BeH	**TS4**	278.7	283.8		279.4	283.2
Bzim···MgH	**Min1**	0.0	0.0	725	0.0	0.0
Bzim···MgH	**Min2**	38.8	41.7	686	18.4	21.2
Bzim···MgH	**Min3**	58.8	63.3	666	40.9	45.2
Bzim···MgH	**TS1**	0.0	0.0		21.8	29.4
Bzim···MgH	**TS2**	72.8	78.0		53.3	59.1
Bzim···MgH	**TS3**	228.5	233.3		228.7	233.0
Bzim···MgH	**TS4**	237.4	243.7		238.0	242.6
Bzim···CaH	**Min1**	14.7	16.5	600		
Bzim···CaH	**Min2**	0.0	0.0	614		
Bzim···CaH	**Min3**	*b*	*b*			
Bzim···CaH	**TS1**	14.6	17.0			
Bzim···CaH	**TS2**	*c*	*c*			
Bzim···CaH	**TS3**	200.3	199.1			
Bzim···CaH	**TS4**	211.2	211.8			

[a]The heterolytic bond dissociation enthalpies (kJ mol^{-1}), BDE, for benzimidazole−metal are also included. [b]In the case of the K and CaH derivatives, the geometry with the metal over the benzene ring (**Min3**) evolves to **Min2**. [c]This TS has not been found.

2). There is an evident transference of charge between the metal and the heterocyclic ring: $\Delta Q_{Li} > \Delta Q_{Na} > \Delta Q_{K}$ and $\Delta Q_{Be} > \Delta Q_{Mg} > \Delta Q_{Ca}$. Similarly, the differences of charge transfer between the metals within the same row in the periodic table follow the pattern $\Delta Q_{Be} \gg \Delta Q_{Li}$, $\Delta Q_{Mg} \gg \Delta Q_{Na}$, and $\Delta Q_{Ca} \gg \Delta Q_{K}$, as described before. The charges of the metallic subunits follow the sequence **Min1** > **Min2** > **Min3**, except for the Na systems, where **Min1** and **Min2** show the same charge whereas that of **Min3** is slightly larger.

The analysis of the charge transfer between the occupied orbitals of the benzimidazole subunit toward the empty ones of the metallic fragments are dominated in **Min1** by the N(lp) → metal transfer (Table S5 of the Supporting Information). The stabilizations found for such interaction are almost identical to the corresponding ones in the imidazole derivatives, with the exception of beryllium where a much larger value than previously obtained (560 kJ mol^{-1}) is found. In the case of **Min2** and **Min3**, all the bonds of the five- and six-membered rings have contributions similar to those of the stabilization energy due to the charge transfer. In some of the derivatives, some charge transfer from the lone pairs of the nitrogen atoms toward the empty orbitals of the metallic moiety are found in **Min2**.

The calculated Wiberg bond indices between the metallic atoms and the heavy atoms of the benzimidazole rings are presented in Table S6 of the Supporting Information. The N1−

dx.doi.org/10.1021/jp502443h | J. Phys. Chem. A 2014, 118, 4195−4204

Table 5. NBO Total Charges (e) of the Metal (Li, Na, and K) or Metal−H (Be, Mg, and Ca) in the Complexes and Absolute Charge Transfer (ΔQ) between Imidazole/Metal Subunits Calculated at the B3LYP/6-31+G** Level

complex	geometry	charge M/MH subunit[a]	ΔQ
Bzim···Li	**Min1**	0.93	0.07
Bzim···Li	**Min2**	0.85	0.15
Bzim···Li	**Min3**	0.85	0.15
Bzim···Na	**Min1**	0.93	0.07
Bzim···Na	**Min2**	0.93	0.07
Bzim···Na	**Min3**	0.94	0.06
Bzim···K	**Min1**	0.96	0.04
Bzim···K	**Min2**	0.95	0.05
Bzim···K	**Min3**	*b*	*b*
Bzim···BeH	**Min1**	0.70	0.30
Bzim···BeH	**Min2**	0.51	0.49
Bzim···BeH	**Min3**	0.49	0.51
Bzim···MgH	**Min1**	0.82	0.18
Bzim···MgH	**Min2**	0.78	0.22
Bzim···MgH	**Min3**	0.77	0.23
Bzim···CaH	**Min1**	0.90	0.10
Bzim···CaH	**Min2**	0.87	0.13
Bzim···CaH	**Min3**	*b*	*b*

[a]Due to the neutral character of the complexes, the total charge of the imidazolates is the same that of the corresponding metal but in negative values. [b]In the case of the K and CaH derivatives, the geometry with the metal over the benzene ring (**Min3**) evolves to **Min2**.

metal bond indexes in **Min1** are almost identical to those found in the analogous imidazole derivatives. In **Min2**, the bond indexes with the N1, C2, and N3 atoms are similar to those of the imidazole derivatives, whereas those with C3a and C7a are less so, calculated as smaller than the corresponding ones in the imidazole derivatives. Thus, the sum of bond indexes in **Min2** for the benzimidazole derivatives is smaller than the corresponding imidazole ones. Finally, in **Min3** similar bond indexes are found between the metallic atoms and all the carbon atoms of the aromatic ring, being slightly larger for the C4−C7 atoms than for the C3a and C7a one. The sum of the bond orders in **Min3** is smaller than in **Min2** for all the derivatives.

The aromaticity indexes in the five- and six-membered rings of the benzimidazole derivatives have been gathered in Table 6. For comparative purposes, the values corresponding to the parent compound and the anion have been included. The NICS values obtained for the five- and six-membered rings range between −13.34 and −9.34 and the HOMA ones between 0.59 and 0.94, corresponding in all cases to a significant aromaticity. The values of the NICS five-membered ring are in general similar to those of the analogous imidazole derivatives, previously discussed, whereas the HOMA values are in general smaller in the benzimidazole derivatives than in the imidazole ones.

The five-membered ring of the alkaline-metal and alkaline-earth-metal derivatives **Min1** and **Min2** configurations show NICS values larger than in the parent compound and smaller than for the isolated anion, except for the Bzim···BeH interaction (**Min1**) where the NICS value is smaller than in the parent compound. **Min3** structures show NICS values slightly more aromatic than in the isolated anion. The NICS values of the six-membered ring in **Min1** are always between

Table 6. NICS(1) and HOMA Aromaticity Indexes in the Five- and Six-Membered Rings of the Benzimidazole Derivatives

	NICS(1)-5	NICS(1)-6	HOMA-5	HOMA-6
Bzim···Li (**Min1**)	−10.96	−10.69	0.80	0.90
Bzim···Li (**Min2**)	−12.01	−10.00	0.76	0.80
Bzim···Li (**Min3**)	−13.31	−10.04	0.69	0.65
Bzim···Na (**Min1**)	−11.27	−10.71	0.81	0.89
Bzim···Na (**Min2**)	−11.50	−10.12	0.77	0.82
Bzim···Na (**Min3**)	−12.68	−9.34	0.73	0.71
Bzim···K (**Min1**)	−11.71	−10.64	0.80	0.87
Bzim···K (**Min2**)	−12.06	−9.95	0.78	0.82
Bzim···BeH (**Min1**)	−9.53	−10.90	0.71	0.94
Bzim···BeH (**Min2**)	−12.07	−9.61	0.74	0.77
Bzim···BeH (**Min3**)	−13.21	−10.26	0.65	0.60
Bzim···MgH (**Min1**)	−10.44	−10.81	0.77	0.92
Bzim···MgH (**Min2**)	−11.11	−10.04	0.74	0.80
Bzim···MgH (**Min3**)	−13.34	−9.62	0.66	0.59
Bzim···CaH (**Min1**)	−11.37	−10.75	0.79	0.90
Bzim···CaH (**Min2**)	−11.87	−10.10	0.77	0.81
Bzim−H	*−10.21*	*−11.05*	0.80	0.93
Bzim (anion)	*−12.50*	*−10.40*	0.79	0.82

those of the parent compound and the anion, whereas the values of **Min2** and **Min3** are slightly smaller than those of the anion and the parent compound.

The HOMA values of the five- and six-membered rings follow the order **Min1** > **Min2** > **Min3**, except for the Bzim··· BeH complex (**Min1**), which is smaller than **Min2**. In addition the values of the HOMA parameters in the six-membered rings are larger than in the five-membered ones in the **Min1** and **Min2** structures whereas the opposite is observed for **Min3**.

3.2.3. Electron Density Analysis. The topological analysis of the electron density of these structures presents a different pattern for each of the stationary points found (Figure 7 and Table S1 of the Supporting Information). Using the Li complexes as an example, the picture shows a simple interaction through the metal and one of the imidazole nitrogen atoms for **Min1** and **TS1**. **Min2** presents three bond paths connecting the metal with the carbon atoms C2, C4a, and C8a. The corresponding ring (rcp) and cage (ccp) critical points (yellow and green points in the figure) are also observed. It is interesting to notice the proximity of the Li−C4a and Li−C8a bcps and the corresponding rcps. In fact, in the molecular graph of the beryllium minimum, all of them collapse in the position of the rcp that is situated in the symmetry plane. **TS2** presents a different pattern, connecting the Li metal with the C4a−C8a bcp by a single path. **Min 3** shows two bcps, two rcp, and one ccp surrounding the metal atom. It should be noted that the ccp and one of the rcp are only possible if two additional bcps corresponding to the Li−C4a and Li−C8a collapse in the position where the rcp is shown. Finally **TS3** and **TS4** present two interactions between the lithium atom and the surrounding hydrogen atoms.

The characteristics of the bcps where metallic atoms are involved are similar to those already discussed for the imidazole derivatives (Table S7 of the Supporting Information). The values of the electron density at the bcps range between 0.118 and 0.005 au and the values of the Laplacian are always positive. In the case of the beryllium bonds, negative values of the total energy H are found whereas in the rest of the cases they are positive. As found previously, the largest values of the electron

dx.doi.org/10.1021/jp502443h | J. Phys. Chem. A 2014, 118, 4195−4204

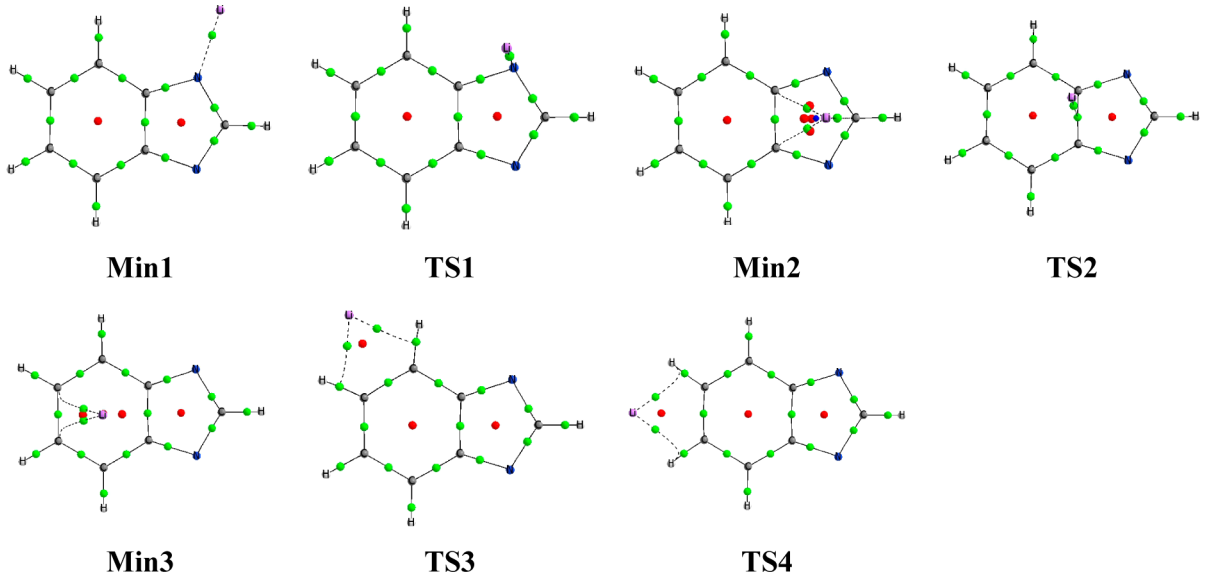

Figure 7. Molecular graph of the unique stationary points of the Bzim−Li potential energy surface.

density and Laplacian at the M−X bcps (where X is any atom of the benzimidazole ring) correspond to the N−M in **Min1**.

3.3. CSD Search. To cross validate our findings with experimental evidence for the existence of neutral π−imidazolate salts, we decided to carry out a search in the CSD[26] for such alkaline-metal and alkaline-earth-metal derivatives. We found that the majority of the systems present the interaction between the metal and the nitrogen of the imidazolate (N−σ bonding) and only six cases correspond to the alkaline-metal (Cs) or alkaline-earth-metal (Ba and Sr) cations interacting with the π-face of the imidazolate ring (Table 7). In some of the cases, the N−σ and πbonding are observed in the same crystal (XEHQAE, XEHQEI, and XEHQOS) (Figure 8).

Table 7. CSD Crystals Structures with π-Bonding and the Distance between the Metallic Atom and the Center of the Imidazolate Ring

CSD refcode	metal atom (M)	M···imidazolate, Å
UCUJOR	Cs	3.099, 3.151
UCUJUX	Cs	3.293, 3.260
XEHQEI	Sr	2.678
CAVTUQ	Ba	2.952, 2.976
XEHQAE	Ba	2.750
XEHQOS	Ba	2.780, 2.768

Expanding our investigation to include other pentagonal aromatic anions, we calculated neutral complexes with the cyclopentadienide anion, the simplest and most symmetric model, at the B3LYP/6-311++G(3df,2p),LanL2DZ level. A search was then performed in the CSD for alkaline-metal and alkaline-earth-metal neutral complexes of pyrrolate and pyrazolate anions using as a cutoff that none of the ring atoms (C and N) should be at a distance longer than 3.5 Å from the metal. Our search was not limited to these three azoles, but there were no examples involving triazoles and tetrazoles as a π-bond donors toward alkaline-metal and alkaline-earth-metal cations within the distance limitation proposed.[26] All the data we have obtained are reported in Table 8.

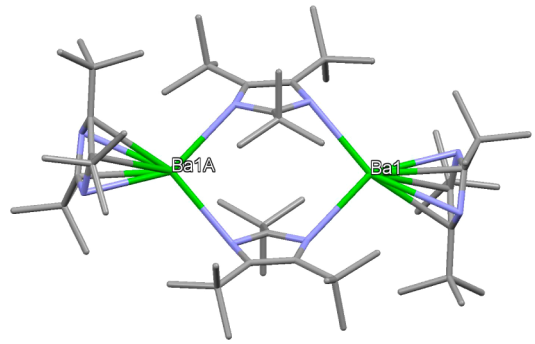

Figure 8. X-ray structure of XEHQAE. The hydrogen atoms have been removed for clarity.

The theoretically calculated M···centroid distances of the Cp are linearly related to the metallic radii (eq 1). The least well correlated values correspond to Li and Ba, for which the predicted radii are 1.44 and 2.38 Å (instead of 1.52 and 2.22 Å). With experimental values, an equation similar to eq 1 but with a slope of 1.333 Å has been reported.[33]

$$d = (1.22 \pm 0.02)\ \text{radii},\ n = 10,\ R^2 = 0.998 \quad (1)$$

The data of Table 8 have been analyzed using a presence−absence matrix[34] for the three heterocycles, Cp being the reference (eq 2).

$$d = (0.34 \pm 0.11) + (0.14 \pm 0.05)\ \text{pyrrolate} + (0.12 \pm 0.07)\ \text{imidazolate} + (0.24 \pm 0.05)\ \text{pyrazolate} + (1.05 \pm 0.06)\ \text{radii},\ n = 16,\ R^2 = 0.955 \quad (2)$$

All the distances are longer with heterocycles than with Cp, and they increase in the order imidazolate ≤ pyrrolate < pyrazolate, the effect of the metallic radii being the dominant factor. Although imidazolates have distances shorter than or equal to those of pyrrolates, their number of examples is considerably lower (Table 8), this could be due, at least partially, to a decreased competitiveness toward N−σ bonding. Thus, notwithstanding, it should be expected that new

dx.doi.org/10.1021/jp502443h | J. Phys. Chem. A 2014, 118, 4195−4204

Table 8. Calculated and Experimental Mean Values Metal···Centroid Distances, d (Å)[a]

metal	cyclopentadienide (Cp)	pyrrolate	imidazolate	pyrazolate	metallic radii (Å)[b]
Li	1.716	2.19 (123)	no data	no data	1.52
Na	2.206	2.57 (66)	no data	2.63 (15)	1.86
K	2.597	2.88 (126)	no data	2.99 (37)	2.27
Rb	2.911	3.01 (1)	no data	no data	2.48
Cs	3.143	3.16 (2)	3.20 (4)	no data	2.65
Be	1.484	no data	no data	no data	
Mg	2.001	2.63 (1)[c]	no data	2.84 (1)[d]	1.60
Ca	2.359	2.51 (7)	no data	2.57 (4)	1.97
Sr	2.626	2.60 (4)	2.68 (1)	2.76 (4)	2.15
Ba	2.825	2.87 (15)	2.85 (5)	2.94 (8)	2.22

[a]In parentheses are the number of cases. In addition, the corresponding metallic radii have been included. Calculated values at B3LYP/6-311++G(3df,2p),LanL2DZ. All the complexes present C_{5v} symmetry and have been verified to be minima at the calculated level. [b]From ref 32. [c]It corresponds to the CSD refcode NAQZEM. [d]It corresponds to the CSD refcode KAFCAX.

examples of neutral metal (groups 1 and 2)···imidazolate π-bonded complexes will soon appear.

4. CONCLUSIONS

A theoretical study of the potential energy surface (minima and transition states) of the neutral complexes formed by alkaline-metal and alkaline-earth-metal derivatives of imidazole and benzimidazole have been carried out by means of B3LYP and G3B3 computational methods. Two minima have been found in the derivatives of imidazole, one with the metal atom interacting with one of the nitrogen atoms and the other interacting with the π-system. Three transition state structures have been characterized that connect these minima. In the case of the benzimidazole, three nondegenerate minima and four TS have been found. The most stable minima of the alkaline-metal derivatives of both systems correspond to the metal interacting with the π-system of the imidazole ring, whereas in the alkaline-earth-metal derivatives, the preferred minima depend on the substituent. Several of the barriers obtained for the transformation of one structure in another are very small, which indicates that these complexes can easily adopt one or another configuration, allowing for metal-jumping. A CSD search has confirmed that the two bonding modes, N−σ and π, are present in solid phase. However, the distribution of the two bonding modes, the N−σ being predominant in solid phase, indicates an important effect of the environment in the stability of the minimum conformations.

■ ASSOCIATED CONTENT

Supporting Information

Molecular graphs and geometry of all the stationary points (minima and TS) calculated at the B3LYP/6-31+G(d,p) and B3LYP/6-311+G(3df,2p) computational levels. NBO second-order perturbation, Wiberg bond indexes, and electron density properties at the bcp's. This material is available free of charge via the Internet at http://pubs.acs.org.

■ AUTHOR INFORMATION

Corresponding Author

*I. Alkorta: e-mail, ibon@iqm.csic.es; web site, http://are.iqm.csic.es.

Notes

The authors declare no competing financial interest.

■ ACKNOWLEDGMENTS

This work was carried out with financial support from the Ministerio de Economía e Innovación (CTQ2012-35513-C02-02), and the Comunidad Autónoma de Madrid (Project MADRISOLAR2, ref S2009/PPQ-1533) is thanked for continuing support. F.B. thanks the support of the European Commission (Marie-Curie grant, People FP7, Project Reference: 274988). Thanks are given to the CTI (CSIC), CESGA, and Ireland's High-Performance Computing Centre (ICHEC) for allocation of computer time. The Trinity Biomedical Sciences Institute is supported by infrastructure funding from Cycle 5 of the Irish Higher Education Authority's Program for Research in Third Level Institutions.

■ REFERENCES

(1) Dougherty, D. A. Cation-π Interactions in Chemistry and Biology: A New View of Benzene, Phe, Tyr, and Trp. *Science* **1996**, *271*, 163−168.

(2) Hunter, C. A.; Lawson, K. R.; Perkins, J.; Urch, C. J. Aromatic Interactions. *J. Chem. Soc., Perkin 2* **2001**, 651−669.

(3) Frontera, A.; Quiñonero, D.; Deyà, P. M. Cation−π and Anion−π Interactions. *Wiley Interdiscip. Rev.: Comput. Mol. Sci.* **2011**, *1*, 440−459.

(4) Rybtchinski, B. Adaptive Supramolecular Nanomaterials Based on Strong Noncovalent Interactions. *ACS Nano* **20fs11**, *5*, 6791−6818.

(5) IUPAC. *Compendium of Chemical Terminology*, 2nd ed. (the "Gold Book"); compiled by McNaught, A. D.; Wilkinson, A. Blackwell Scientific Publications: Oxford, 1997; last update 2010-12-22.

(6) *Histamine and H1-Antihistamines in Allergic Disease*, 2nd ed.; Estelle, F., Simons, R., Eds.; Taylor & Francis: London, 2002.

(7) Gilch, H.; Schweitzer-Stenner, R.; Dreybrodt, W. Structural Heterogeneity of the Fe(2+)-N epsilon (HisF8) Bond in Various Hemoglobin and Myoglobin Derivatives Probed by the Raman-Active Iron Histidine Stretching Mode. *Biophys. J.* **1993**, *65*, 1470−1485.

(8) Banerjee, R.; Ragsdale, S. W. The Many Faces of Vitamin B12: Catalysis by Cobalamin- Dependent Enzymes. *Annu. Rev. Biochem.* **2003**, *72*, 209−247.

(9) (a) McKee, V.; Zvagulis, M.; Dagdigian, J. V.; Patch, M. G.; Reed, C. A. Hemocyanin Models: Synthesis, structure, and magnetic properties of a binucleating copper(II) system. *J. Am. Chem. Soc.* **1984**, *106*, 4765−4772. (b) Stöckel, J.; Safar, J.; Wallace, A. C.; Cohen, F. E.; Prusiner. Prion Protein Selectively Binds Copper(II) Ions. *Biochemistry* **1998**, *37*, 7185−7193. (c) Sharma, R.; Rensing, C.; Rosen, B. P.; Mitra, B. Enzyme catalysis and regulation. *J. Biol. Chem.* **2000**, *275*, 3873−3878. (d) Anderson, M.; Hedin, J.; Johansson, P.; Nordström, J.; Nyfén, M. Coordination of Imidazoles by Cu(II) and Zn(II) as Studied by NMR Relaxometry, EPR, far-FTIR Vibrational Spectroscopy and Ab Initio Calculations: Effect of Methyl Substitution. *J. Phys. Chem. A* **2010**, *114*, 13146−13153.

(10) Dyson, P. J.; Geldbach, T. J. *Metal Catalysed Reactions in Ionic Liquids*; Springer: Dordrecht, The Netherlands, 2005.
(11) (a) Arduengo, A. J., III; Harlow, R. L.; Kline, M. A stable crystalline carbine. *J. Am. Chem. Soc.* **1991**, *113*, 361−363. (b) Arduengo, A. J., III; Goerlich, J. R.; Marshall, W. J. A stable diaminocarbene. *J. Am. Chem. Soc.* **1995**, *117*, 11027−11028. (c) Arduengo, A. J., III; Davidson, F.; Dias, H. V. R.; Goerlich, J. R.; Khasnis, D.; Marshall, W. J.; Prakasha, T. K. An Air Stable Carbene and Mixed Carbene "Dimers. *J. Am. Chem. Soc.* **1997**, *119*, 12742−12749. (d) Arduengo, A. J., III. Looking for Stable Carbenes: The Difficulty in Starting Anew. *Acc. Chem. Res.* **1999**, *32*, 913−921. (e) Arduengo, A. J., III; Tapu, D.; Marshall, W. J. A Bimetallic Complex Containing a Cyclopentadienyl-Annulated Imidazol-2-ylidene. *J. Am. Chem. Soc.* **2005**, *127*, 16400−16401. (f) Dixon, D. A.; Arduengo, A. J., III. Accurate Heats of Formation of the "Arduengo-Type" Carbene and Various Adducts Including H2 from ab Initio Molecular Orbital Theory. *J. Phys. Chem. A* **2006**, *110*, 1968−1974.
(12) Cortes-Llamas, S. A.; Hernandez-Lamoneda, R.; Velazquez-Carmona, M. A.; Munoz-Hernandez, M. A.; Toscano, R. A. 3,5-Dimethyl and 3,5-Di-tert-butylpyrazolato Complexes with Alkali Metals: Monomeric, Dimeric, Cluster, and 1D Chain Structures. *Inorg. Chem.* **2006**, *45*, 286−294.
(13) Cortes-Llamas, S.; Velazquez-Carmona, M. A.; Munoz-Hernandez, M. A. Isolation and Authentication of a Sodium Bispyrazolylaluminate. *Inorg. Chem. Commun.* **2005**, *8*, 155−158.
(14) Blanco, F.; Alkorta, I.; Elguero, J. The Structure of Alkali Metal Derivatives of Azoles: N−σ versus π Structures. *J. Phys. Chem. A* **2008**, *112*, 7682−7688.
(15) Blanco, F.; Alkorta, I.; Elguero, J. N-sigma versus π Configuration in Mono- and bis-Pyrrole and Imidazole Derivatives of Alkaline Earth Metals. *J. Phys. Org. Chem.* **2009**, *22*, 747−755.
(16) Ma, J. C.; Dougherty, D. A. The Cation−π Interaction. *Chem. Rev.* **1997**, *97*, 1303−1324.
(17) Frisch, M. J.; Trucks, G. W.; Schlegel, H. B.; Scuseria, G. E.; Robb, M. A.; Cheeseman, J. R.; Montgomery, J. A., Jr.; Vreven, T.; Kudin, K. N.; Burant, J. C.; Millam, J. M.; Iyengar, S. S.; Tomasi, J.; Barone, V.; Mennucci, B.; Cossi, M.; Scalmani, G.; Rega, N.; Petersson, G. A.; Nakatsuji, H.; Hada, M.; Ehara, M.; Toyota, K.; Fukuda, R.; Hasegawa, J.; Ishida, M.; Nakajima, T.; Honda, Y.; Kitao, O.; Nakai, H.; Klene, M.; Li, X.; Knox, J. E.; Hratchian, H. P.; Cross, J. B.; Bakken, V.; Adamo, C.; Jaramillo, J.; Gomperts, R.; Stratmann, R. E.; Yazyev, O.; Austin, A. J.; Cammi, R.; Pomelli, C.; Ochterski, J. W.; Ayala, P. Y.; Morokuma, K.; Voth, G. A.; Salvador, P.; Dannenberg, J. J.; Zakrzewski, V. G.; Dapprich, S.; Daniels, A. D.; Strain, M. C.; Farkas, O.; Malick, D. K.; Rabuck, A. D.; Raghavachari, K.; Foresman, J. B.; Ortiz, J. V.; Cui, Q.; Baboul, A. G.; Clifford, S.; Cioslowski, J.; Stefanov, B. B.; Liu, G.; Liashenko, A.; Piskorz, P.; Komaromi, I.; Martin, R. L.; Fox, D. J.; Keith, T.; Al-Laham, M. A.; Peng, C. Y.; Nanayakkara, A.; Challacombe, M.; Gill, P. M. W.; Johnson, B.; Chen, W.; Wong, M. W.; Gonzalez, C.; Pople, J. A. *Gaussian-03*; Gaussian, Inc.: Wallingford, CT, 2003.
(18) Baboul, A. G.; Curtiss, L. A.; Redfern, P. C.; Raghavachari, K. G3(B3) and G3(MP2B3). *J. Chem. Phys.* **1999**, *110*, 7650.
(19) Bader, R. F. W. *Atoms in Molecules: A Quantum Theory*; Clarendon Press: Oxford, U.K., 1990.
(20) Biegler-König, F. W.; Bader, R. F. W.; Tang, T. H. Calculation of the Average Properties of Atoms in Molecules. II. *J. Comput. Chem.* **1982**, *3*, 317−328.
(21) Biegler-König, F. W.; Schönbom, J. *AIM2000*, 2.0 ed.; Buro Streibel Biegler-König: Bielefeld, Germany, 2002; http://www.aim2000.de/.
(22) Keith, Todd A. *AIMAll*, Version 13.11.04; TK Gristmill Software: Overland Park, KS, USA, 2013' aim.tkgristmill.com.
(23) Krygowski, T. M. Crystallographic Studies of Inter- and Intramolecular Interactions Reflected in Aromatic Character of.pi.-Electron Systems. *J. Chem. Inf. Comput. Sci.* **1993**, *33*, 70−78.
(24) Schleyer, P. V.; Maerker, C.; Dransfeld, A.; Jiao, H. J.; Hommes, N. J. R. V. Nucleus-Independent Chemical Shifts: A Simple and Efficient Aromaticity Probe. *J. Am. Chem. Soc.* **1996**, *118*, 6317−6318.
(25) Schleyer, P. V.; Manoharan, M.; Wang, Z. X.; Kiran, B.; Jiao, H. J.; Puchta, R.; Hommes, N. J. R. V. Dissected Nucleus-Independent Chemical Shift Analysis of π-Aromaticity and Antiaromaticity. *Org. Lett.* **2001**, *3*, 2465−2468.
(26) Allen, F. H. Cambridge Structural Database: a Quarter of a Million Crystal Structures and Rising . *Acta Crystallogr.* **2002**, *B58*, 380−388.
(27) Alkorta, I.; Blanco, F.; Elguero, J.; Claramunt, R. M. *Tetrahedron* **2010**, *66*, 2863−2868.
(28) Alkorta, I.; Popelier, P. L. A. Computational Study of Mutarotation in Erythrose and Threose. *Carbohydr. Res.* **2011**, *346*, 2933−2939.
(29) Azofra, L.; Alkorta, I.; Elguero, J.; Popelier, P. L. A. Conformational Study of the Open-Chain and Furanose Structures of D-Erythrose and D-Threose. *Carbohydr. Res.* **2012**, *358*, 96−105.
(30) Yáñez, M.; Mó, O.; Alkorta, I.; Elguero Can, J. Conventional Bases and Unsaturated Hydrocarbons Be Converted into Gas-Phase Superacids That Are Stronger than Most of the Known Oxyacids? The Role of Beryllium Bonds. *Chem.—Eur. J.* **2013**, *19*, 11637−11643.
(31) Mó, O.; Yáñez, M.; Alkorta, I.; Elguero, J. Modulating the Strength of Hydrogen Bonds through Beryllium Bonds. *J. Chem. Theory Comput.* **2012**, *8*, 2293−2300.
(32) Greenwood, N. N.; Earnshaw, A. *Chemistry of the Elements*, 2nd ed.; Elsevier-Butterworth-Heinemann: Amsterdam, 1997.
(33) Sockwell, S. C.; Hanusa, T. P. Detection of Covalency in Cyclopentadienyl Complexes of the Alkaline-Earth and f Elements: Statistical Evaluation of Structural Data. *Inorg. Chem.* **1990**, *29*, 76−80.
(34) Alkorta, I.; Blanco, F.; Elguero, J. A theoretical structural analysis of the factors that affect $^{1}J_{NH}$, $^{1h}J_{NH}$ and $^{2h}J_{NN}$ in N−H···N hydrogen-bonded complexes. *Magn. Reson. Chem.* **2009**, *47*, 249−256.